Separation Of Conglomerate Forming Enantiomers Using A Novel Continuous Preferential Crystallization Process

Thomas Vetter*[1], Christopher L. Burcham[2] and Michael F. Doherty[3]

[1]School of Chemical Engineering and Analytical Science, University of Manchester, Manchester, United Kingdom

[2]Eli Lilly & Company, Indianapolis, Indiana 46285

[3]Department of Chemical Engineering, University of California, Santa Barbara, California 93106

Abstract

Providing enantiomerically pure products is of key importance in the fine chemicals, food and pharmaceutical industries. In this article, a continuous preferential crystallization process is presented that allows the separation of conglomerate forming enantiomers in a stable, robust and flexible way. This is achieved by coupling two continuous

This article is dedicated to John M. Prausnitz for his many outstanding contributions to solution thermodynamics and phase equilibria. The new continuous process reported here is based on the properties of ternary phase diagrams for conglomerate forming enantiomers dissolved in solution.

*Correspondence concerning this article should be addressed to T. Vetter at thomas.vetter@manchester.ac.uk

crystallizers by exchanging their clear liquid phases. Each crystallizer is connected to a suspension mill responsible for in-situ seed generation through particle breakage. The dynamic and steady state behavior of this process is extensively analyzed for racemic feed streams through process simulations, and parameter regions, which yield pure enantiomers in both crystallizers, are identified. For enriched feed streams we further show when this novel flowsheet is capable of outperforming an ideal batch process in terms of solvent consumption per unit mass of desired enantiopure product produced.

Keywords. separation of enantiomers; continuous crystallization; milling; population balance equation models; process design; threonine

Introduction

Obtaining enantiopure products is important in many industries, e.g., the pharmaceutical, food and fine chemicals industries. In a pharmaceutical product typically only one of the enantiomers is biologically active, while the other enantiomer is either not effective as a drug or even harmful to humans. In such cases, the pharmaceutical industry strives to produce enantiomerically pure compounds. Two major routes to enantiopure products are evident: asymmetric chemical synthesis or the separation of enantiomers from an enantiomerically impure starting material. While the former is the more desirable option in terms of raw material consumption, it often does not allow attaining the required purity directly. Therefore, the development of processes that allow separating enantiomers is essential.

The two major separation process alternatives in this context are continuous chiral chromatography[1,2] and crystallization processes[3,4]. An overview of further resolution methods is given in a recent review article by Lorenz and Seidel-Morgenstern[5]. The product resulting from chromatography is a liquid, however, most products in the pharmaceutical, food and fine chemicals industries are ultimately sold as solids. Hence, there is usually a further crystallization step necessary to obtain the desired solid particles with high purity. On the other hand, the most commonly used crystallization-based resolution process relies on the formation of two diastereomeric salts that have different physical properties and can thus be crystallized consecutively[6–8]. However, this process requires the molecules to form salts, which is not always possible. It also requires (at least) stoichiometric amounts of a

chiral resolving agent, which needs to be separated from the desired product and recycled in further processing steps.

From a standpoint of process intensification, specifically the minimization of energy requirements and solvent consumption, it is appealing to investigate crystallization processes that can separate enantiomers and deliver a solid product in a single process step from a solution containing both enantiomers and a solvent[4]. The crystallization strategy to be employed mainly depends (1) on the type of phase diagram for a specific ternary system, (2) whether racemization in solution is possible, and (3) the enantiomeric excess in the feed material[5,9]. Most ternary phase diagrams of organic enantiomers and a solvent correspond to one of three classes: conglomerates, racemic compound forming systems and solid solutions[10]. Qualitative ternary phase diagrams for these three cases are shown in Figure 1 in the form of isothermal cuts. In that figure, we have indicated the type and number of stable phases in each phase region. The key difference between the different types of phase diagrams lies in the structure of the solid phases that can be obtained. In conglomerates (Figure 1a, around 10% of all cases) the stable crystalline phases consist of either pure S enantiomer or pure R enantiomer. In racemic compound forming systems (Figure 1a, around 90% of all cases), there is additionally a solid racemic compound that consists of equal amounts of R and S enantiomer (designated RS). Fortunately, the case of solid solutions (Figure 1c), where crystals can contain any composition of R and S enantiomers and which are hardest to separate[11], is rarely encountered for organic molecules. Apart from the ideal cases shown in Figure 1 there are numerous (combinations of) nonidealities possible, e.g., the presence of a

metastable conglomerate in racemic compound forming systems[12], partial solid solutions[13], the presence of liquid-liquid equilibria[14], and the presence of (metastable) polymorphs[15].

In this article we will focus our attention on conglomerates. If the enantiomeric excess in the feed material is high enough, direct crystallization in the two phase region is possible. This is shown on the right side of Figure 2a for an isothermal batch crystallization. In this process, one starts from a supersaturated initial condition (green circle) and upon nucleation or the introduction of seed crystals of the R enantiomer, one follows the mass balance line (dashed grey line) to the thermodynamic equilibrium (blue square). Clearly, a continuous crystallization process carried out in a mixed suspension, mixed product removal crystallizer (MSMPRC) with feed conditions in the two phase region (green circle in Figure 2b) reaches a steady state operating point (blue square) that lies in the two phase region as well. It is therefore able to produce pure R enantiomer in a continuous fashion.

When there is no enantiomeric excess in the feed material, preferential crystallization[16] is one of the most attractive processing alternatives[‡]. The two key concepts that enable preferential crystallization processes are (1) the dependence of mass uptake of solute into the crystalline phase on the surface area of the crystals, i.e., the amount of solute incorporated per unit time depends linearly on the total surface area of the crystals present in the suspension, and (2) the existence of a metastable zone, i.e., the nucleation of new crystals (in this case of the counter-enantiomer) is an activated pro-

[‡]Note that we are primarily interested in cases where racemization of enantiomers in the solution proves difficult. In cases where racemization in solution is more accessible the process of Viedma ripening[17–20] becomes relevant.

cess and does not readily occur at low supersaturations. In the case of a conglomerate, it therefore becomes possible to preferentially grow crystals of the desired enantiomer through a seeded process. Performing this process in a batch crystallizer at constant temperature (as shown in the three phase region of Figure 2a), the initially racemic and supersaturated liquid phase (green circle) is depleted of the R enantiomer, which continues until nuclei of the undesired S enantiomer are formed (at this time the process trajectory of the residual liquid composition breaks away from the dashed line). Henceforth, the solution rapidly approaches the thermodynamic equilibrium, i.e., it becomes racemic again, but at the saturation concentration (purple square symbol). An isothermal batch crystallization process based on preferential crystallization would be stopped before the nucleation of crystals of the undesired enantiomer occurs, so that only pure crystals of the desired enantiomer can be collected. Since such a precise stopping of the crystallization process and a quick filtration of the product crystals is cumbersome, preferential crystallization processes can be carried out in a polythermal fashion as described by Levilain and Coquerel [21] and Levilain et al. [22].

Recently, advanced continuous processing concepts that allow preferential crystallization processes to be operated at steady state have been developed [22–25]. In this article, we add to these concepts by presenting a novel processing flowsheet and its rationale (in section "The flowsheet and its rationale"). This flowsheet allows operating continuous preferential crystallization processes for a wide range of kinetics (even for cases with a narrow metastable zone for the undesired enantiomer) and with a high yield. This

is accomplished through the use of mother liquor recycles (to increase the yield) and heated suspension mills (to generate seed crystals in-situ by breaking parent particles and to dissolve nuclei of the undesired enantiomer) as described in the next section. We then construct a process model based on population balance equations (in section "Process model") that allows us to evaluate the dynamic and steady state behavior of the process. In the results and discussion section we will show through extensive process simulations that the flowsheet can be operated in an inherently stable fashion, i.e., that steady states can be found that are approached even from enantiomerically impure initial conditions. The ranges of process parameters where this behavior is observed are then identified. For the case of enriched feed streams, we identify the conditions where our novel continuous flowsheet is able to produce pure enantiomers with lower solvent requirements than an ideally operated batch crystallization process.

The flowsheet and its rationale

Levilain and Coquerel[21] described how a single batch crystallizer can be used to obtain the desired enantiomer in a safe and reproducible manner by first crystallizing it as described above and then raising the temperature to dissolve crystals of the undesired enantiomer (and part of the crystals of the desired enantiomer). This concept was subsequently expanded by Levilain et al.[22] using two crystallizers in order to couple preferential crystallization and dissolution. Since these crystallizers were initially seeded with opposite enantiomers, the process allowed obtaining both enantiomers in pure form.

While such processes where an improvement to the rather unstable batch operation as described in the introduction (text relating to Figure 2a), an important fact was not accounted for: preferential crystallization processes are ideal to be run continuously. The continuous operation of preferential crystallization has the advantage that these kinetically controlled processes can be run at a steady state away from the thermodynamic equilibrium, such that the desired enantiomer is obtained continuously with a high purity and a high yield. A continuous preferential crystallization process was first presented in the open literature by Qamar et al. [23]. They treated a single mixed suspension mixed product removal crystallizer (MSMPRC) with a fines dissolution pipe and numerically investigated the effect of different ratios of residence times (main crystallizer vs. dissolution pipe) and different seeding strategies, i.e., seeds were either introduced continuously or in periodic fashion through the feed stream. In a follow-up paper a flowsheet with two coupled crystallizers, which were seeded using opposite enantiomers and which were connected through liquid phase exchange pipes, was presented. [24] This concept was previously successfully demonstrated — both theoretically and experimentally — for two coupled batch crystallizers [26,27] As in the case of the two batch crystallizers, the continuous process allowed obtaining both enantiomers in pure form. The continuous process is schematically drawn inside the three phase region of the isothermal phase diagram shown in Figure 2b. In that figure, the green circle represents the feed point, while the square and triangle represent the steady states of the two coupled crystallizers. The exchange of the liquid phase between the two crystallizers mimics its racemization, i.e., the higher the exchange rate between the two crys-

tallizers, the closer move the square and triangle to the vertical center line (indicated by the arrows in that figure). The effect of this exchange is an increase in the supersaturation of the preferred enantiomer and decrease in the supersaturation of the undesired enantiomer in each crystallizer, hence leading to a better performance of the process and a broader operating window of the process. However, Qamar et al.[23],[24] still used continuous or periodic seeding to accomplish their separation performance (in the case of Qamar et al.[24] seed crystals for both enantiomers were needed). An experimental implementation of a similar process was presented by Chaaban et al.[28],[29], who, however, only treated the liquid phase in a continuous fashion and needed to restart their process with fresh seeds after some time. Furthermore, the yield obtained from all three processes was rather low.

In this paper, we present a novel flowsheet for continuous preferential crystallization with an increased productivity, in-situ seed generation by particle breakage and an even broader operating window. The overall flowsheet of such a process is drawn in Figure 3. Similar to Qamar et al.[24] the two MSMPRCs are fed from a single feed tank with a clear racemic solution and the two crystallizers exchange liquid phase with each other. However, there are two main novelties in our flowsheet: (1) the use of heated mills for in-situ seed generation and fines dissolution and (2) the inclusion of continuous filtration units and recycle streams for the mother liquor separated in the filtration units to increase the process yield. Introducing the suspension mills as shown in Figure 3 enables the in-situ production of seeds by breaking parent particles entering the mills from their respective crystallizers. Naturally, other devices that generate additional crystals from parent particles,

such as sonicators, could be used for this purpose as well. Furthermore, operating the mills at an elevated temperature enables the dissolution of fines particles of the undesired enantiomer, possibly generated by nucleation in the crystallizer. This last point is of key importance because the supersaturation of the undesired enantiomer in each crystallizer is *necessarily* higher than for the desired enantiomer unless the liquid phases between the two crystallizers are exchanged at infinitely fast rates, which would lead to total racemization of the liquid phase in each crystallizer. However, this is clearly impossible due to physical constraints on the exchange flow rates between the two crystallizers. Since the supersaturation of the undesired enantiomer is higher, its (homogeneous) nucleation rate must be faster as well. For systems with a narrow metastable zone of the undesired enantiomer this fact becomes problematic, because there is a substantial risk that nuclei of the undesired enantiomer accumulate over time in each crystallizer, such that the system leaves its previous, apparently stable, state rapidly. Ultimately, this would lead to enantiomerically impure products. Our use of suspension mills at an elevated temperature is therefore expected to remove this issue and stabilize the process by generating a large amount of seeds by breaking particles of the desired enantiomer and by dissolving nuclei of the undesired enantiomer.

In the following two sections, we will present a process model based on the population balance equation (in section "Process model") and then investigate, through the use of a copious amount of process simulations at various conditions, whether our rationalization of the flowsheet is accurate (in section "Results and discussion").

Process model

In order to describe the evolution of the particle size distribution of both enantiomers in all processing units population balance equations (PBEs) are used[30,31], which are coupled with mass balances for the liquid phase. We assume that a single characteristic length can describe the particles, that the crystallizers (C) and mills (M) are well mixed, and that no size classification occurs at their outlets, so that the particle size distribution in the stream leaving the processing unit is the same as the particle size distribution inside the processing unit. The process model detailed below is solved using a high resolution finite volume scheme as described by Gunawan et al. [32], which has been implemented in MatLAB 2014b[33].

Crystallizer

Additional to the assumptions outlined above, we will assume that no agglomeration and breakage of particles occurs in the crystallizer. With reference to the overall flowsheet (cf. Figure 3), the population balance equation for the crystallizer can then be written as

$$\frac{\partial n^j_{\mathrm{C}i}(L,t)}{\partial t} = -\frac{\partial\left(G(S^j_{\mathrm{C}i},T_{\mathrm{C}i},L)n^j_{\mathrm{C}i}(L,t)\right)}{\partial L} + \\ + \frac{1}{m_{\mathrm{C}i}}\left(\dot{m}_{\mathrm{M}i\mathrm{C}i}n^j_{\mathrm{M}i}(L,t) - \dot{m}_{\mathrm{C}i\mathrm{M}i}n^j_{\mathrm{C}i}(L,t) - \dot{m}_{\mathrm{C}i\mathrm{F}i}n^j_{\mathrm{C}i}(L,t)\right) \tag{1}$$

where $n^j_{\mathrm{C}i}(L,t)$ is the number density distribution of particles of enantiomer $j \in \{\mathrm{R};\mathrm{S}\}$ per unit mass of suspension in crystallizer $i \in \{1;2\}$, L is the characteristic length of particles, t is the time, G is the crystal growth rate

of the particles, $S^j_{\mathrm{C}i}$ is the supersaturation with respect to enantiomer j in crystallizer i, and $T_{\mathrm{C}i}$ is the temperature in crystallizer i. The first term on the r.h.s. of Eq. (1) therefore describes the growth kinetics in the crystallizer, while the further terms characterize the in- and out-flows of particles to and from the crystallizer. The flow terms are written using the mass flow rates and the mass of suspension in the crystallizer, e.g., $\dot{m}_{\mathrm{M}i\mathrm{C}i}$ is the mass flow rate from mill i to crystallizer i and $m_{\mathrm{C}i}$ is the mass of suspension in crystallizer i (including any solids and liquid). The supersaturation is defined by:

$$S^j_{\mathrm{C}i} = \frac{c^j_{\mathrm{C}i}}{c^j_{\star,\mathrm{C}i}(T, c^p_{\mathrm{C}i})} \tag{2}$$

where $c^j_{\mathrm{C}i}$ is the concentration of enantiomer j in crystallizer i. The solubility of enantiomer j is designated by $c^j_{\star,\mathrm{C}i}(T, c^p_{\mathrm{C}i})$, where the superscript p represents the counter-enantiomer (i.e., $p = \mathrm{R}$ for $j = \mathrm{S}$ and vice versa). Note that in Eq. (1) we have assumed that the recycle stream originating from the filtration unit and the exchange stream originating from the other crystallizer are particle free and thus do not appear in the PBE. The initial, boundary and regularity conditions for Eq. (1) can be written as:

$$\begin{aligned} n^j_{\mathrm{C}i}(L, t=0) &= n^j_{0,\mathrm{C}i}(L) \\ n^j_{\mathrm{C}i}(L=0, t) &= \frac{J(S^j_{\mathrm{C}i}, T_{\mathrm{C}i})}{G(S^j_{\mathrm{C}i}, T_{\mathrm{C}i}, L=0)} \\ n^j_{\mathrm{C}i}(L=\infty, t) &= 0 \end{aligned} \tag{3}$$

where J is the nucleation rate per unit mass of clear liquid and $n^j_{0,\mathrm{C}i}(L)$ is the number density distribution per unit mass of suspension of the seed

crystals of enantiomer j in crystallizer i. In order to track the evolution of the supersaturation of both enantiomers in the crystallizer, the population balance equation is coupled with a mass balance for the liquid phase:

$$\begin{aligned}\frac{\mathrm{d}c^j_{\mathrm{C}i}}{\mathrm{d}t} =& - k_v\rho_c\frac{\mathrm{d}\mu^j_{3,\mathrm{C}i}}{\mathrm{d}t} + \frac{1}{m_{\mathrm{C}i}}\left(\dot{m}_{\mathrm{SC}i}c^j_{\mathrm{S}} + \dot{m}_{\mathrm{M}i\mathrm{C}i}c^j_{\mathrm{M}i} + \dot{m}_{\mathrm{C}q\mathrm{C}i}c^j_{\mathrm{C}q} + \dot{m}_{\mathrm{F}i\mathrm{C}i}c^j_{\mathrm{F}i}\right) + \\ & - \frac{1}{m_{\mathrm{C}i}}\left(\dot{m}_{\mathrm{C}i\mathrm{C}q}c^j_{\mathrm{C}i} + \dot{m}_{\mathrm{C}i\mathrm{M}i}c^j_{\mathrm{C}i} + \dot{m}_{\mathrm{C}i\mathrm{F}i}c^j_{\mathrm{C}i}\right)\end{aligned} \tag{4}$$

where the concentration of enantiomer j in crystallizer i ($c^j_{\mathrm{C}i}$) is defined per mass of clear liquid and we use the subscript q for streams originating from the other crystallizer (i.e., $q = 2$ for $i = 1$ and vice versa). $\mu^j_{3,\mathrm{C}i}$ is the third moment of the particle size distribution of enantiomer j in crystallizer i, which is defined as

$$\mu^j_{3,\mathrm{C}i} = \int_0^\infty L^3 n^j_{\mathrm{C}i}(L,t)\ \mathrm{d}L \tag{5}$$

The initial condition for Eq. (4) is given by $c^j_{\mathrm{C}i}(t=0) = c^j_{0,\mathrm{C}i}$.

Mill

The population balance equation for the suspension mills can be written in a similar fashion, but includes additional terms describing the appearance

and disappearance of particles due to breakage:

$$\begin{aligned}\frac{\partial n^j_{\mathrm{M}i}(L,t)}{\partial t} =& -\frac{\partial\left(G(S^j_{\mathrm{M}i},T_{\mathrm{M}i},L)n^j_{\mathrm{M}i}(L,t)\right)}{\partial L}+\\ &+\int_L^\infty K(\lambda)d(\lambda,L)n^j_{\mathrm{M}i}(\lambda,t)\mathrm{d}\lambda - K(L)n^j_{\mathrm{M}i}(L,t)+\\ &+\frac{1}{m_{\mathrm{M}i}}\left(\dot{m}_{\mathrm{C}i\mathrm{M}i}n^j_{\mathrm{C}i}(L,t)-\dot{m}_{\mathrm{M}i\mathrm{C}i}n^j_{\mathrm{M}i}(L,t)\right)\end{aligned} \tag{6}$$

where we have assumed that the liquid phase is supersaturated with respect to enantiomer j. If $S^j_{\mathrm{M}i} < 1$, the growth rate G is replaced with the (negative) dissolution rate D, which will cause particles to dissolve/shrink. As mentioned in section "The flowsheet and its rationale", the temperatures in the mills are typically set to induce complete dissolution of nuclei of the undesired enantiomer (and *partial* dissolution of crystals of the desired enantiomer). The milling process itself is characterized through the daughter distribution $d(\lambda, L)$, where $d(\lambda, L)\mathrm{d}L$ is the number of fragments with size between L and $L + \mathrm{d}L$ formed from a larger particle of size λ, and the breakage rate $K(L)$. The initial, boundary and regularity conditions, as well as the mass balance can be formulated similarly to Eqs. (3) and (4), respectively.

Filtration unit

Since this work is not focused on modeling the continuous filtration unit precisely, we make the simplistic assumption that the filtration unit perfectly separates crystals from the mother liquor. As can be seen from the flowsheet in Figure 3 part of the mother liquor is recycled to the crystallizer in order to

increase the overall yield of the process. The remaining part of the mother liquor is purged from the system, therefore preventing the build up of any impurities (and solvent).

Constitutive equations

The above description of the process equations is kept rather general. However, in order to arrive at a specific process example, constitutive equations for the solubility, as well as the growth, dissolution and breakage kinetics are necessary. In this paper a case study on the conglomerate forming system of (2S,3R)- and (2R,3S)-threonine crystallized from water will be presented for which some of the necessary data is already available in the literature. In the equations above and the following considerations, we designate the superscript S to (2S,3R)-threonine and the superscript R to (2R,3S)-threonine. Where appropriate kinetic data is not available from the literature, we specify the assumptions we made to complete the process model. Note that the constitutive equations are the same for both enantiomers, but their arguments (e.g., the supersaturation) differ. The constitutive equations are explained individually in the following sub-sections and are also summarized in Table 1, where all necessary kinetic parameters are included.

Solubility

In order to describe the solubility of both enantiomers in the three phase region of a conglomerate forming system of enantiomers, it is sufficient to know the solubility at racemic composition for different temperatures, $c_{\star,\mathrm{rac}}(T)$. In order to obtain a continuous description, we fitted a second order poly-

nomial through previously reported datapoints[34]:

$$c_{\star,\mathrm{rac}}(T) = k_{c1} + k_{c2}T + k_{c3}T^2 \tag{7}$$

where k_{ci} are parameters. The solubility line for each enantiomer, $c^j_\star(T, c^p)$, is given by the straight line connecting the solubility at racemic composition and the corner of the ternary phase diagram representing the pure enantiomer; as can for example be seen in Figure 1a. It follows that the solubility of enantiomer j depends on the concentration of the counter-enantiomer p.

Crystallization and dissolution kinetics

For the growth and nucleation kinetics, we will largely use the kinetic model for (2S,3R)- and (2R,3S)-threonine reported by Qamar et al.[24], however, since we are primarily interested in the process flowsheet and its features, we have taken the liberty to simplify some of the expressions for convenience. The growth and nucleation kinetics and the relevant kinetic constants are reported in Table 1. For the dissolution kinetics we assumed that they follow a simple linear dependence on the undersaturation

$$D = k_\mathrm{d}\,(S - 1) \tag{8}$$

Breakage kinetics

Crystal breakage occurs in the suspension mills through collisions of crystals with each other and by intensive contacts of the crystals with parts of the mill. Clearly, the specific type and extent of breakage depends on the

type of mill used and its operating parameters. However, for the sake of this study, we assume that particle breakage can be described as a binary breakage process, i.e., original particles break in exactly two fragments, but the fragments are allowed to be of different sizes. Such a breakage process can, for example, be described using a U-shaped daughter distribution that is symmetric in volume space[20]:

$$d(\lambda, L) = 3L^2(2k_{\mathrm{b1}} + 1)\left(\frac{2}{\lambda^3}\right)^{2k_{\mathrm{b1}}+1}\left(L^3 - \frac{\lambda^3}{2}\right)^{2k_{\mathrm{b1}}} \tag{9}$$

where k_{b1} is an integer parameter; the larger the value of k_{b1} the bigger the difference in size between the two fragments formed from the original particle. For our case study we have assumed that $k_{\mathrm{b1}} = 7$, i.e., that the particle breakage is attrition-like. The breakage kinetics are completed by specifying a size-dependent breakage rate, $K(L)$:

$$K(L) = k_{\mathrm{b2}}L^{k_{\mathrm{b3}}} \tag{10}$$

Results and discussion

Racemic feed streams

Determination of steady states and their stability

According to a degree of freedom analysis of the overall flowsheet and following the assumptions made in section "Process model", it is only necessary to specify some of the streams in the flowsheet, while all other quantities can be calculated using the model equations above and additional material

balances over individual process units and parts of the flowsheet. For the purpose of our case study, we choose to specify the following flow rates: the feed flow rate to each crystallizer ($\dot{m}_{\mathrm{SC}i}$), the exchange flow rate between the crystallizers ($\dot{m}_{\mathrm{C}i\mathrm{C}q}$), the flow rate from each crystallizer to its attached mill ($\dot{m}_{\mathrm{C}i\mathrm{M}i}$), as well as the flow rate from each crystallizer to its filtration unit ($\dot{m}_{\mathrm{C}i\mathrm{F}i}$). We also specify the composition of the feed stream (i.e., the mass fraction of both enantiomers, $w^j_{\mathrm{SC}i}$), the size of each processing unit (in terms of the suspension mass it contains, e.g., $m_{\mathrm{C}i}$), as well as the temperature in each processing unit (e.g., $T_{\mathrm{C}i}$).

In order to investigate the behavior of the processing flowsheet in Figure 3, we introduce two case studies with different processing parameters. For the first case study, all processing parameters are introduced in Table 2. Note that we chose to keep the processing parameters for both sides of the flowsheet equivalent, so that only the specifications for the left side (crystallizer 1, etc.) are given in this table. The second case study uses the same processing parameters with the exception of the exchange flow rate between the two crystallizers. In case study 1, we have selected a substantial exchange flow rate between the two crystallizers, while in case study 2 we chose to decouple the two crystallizers by setting the exchange flow rate between them to zero (i.e., $\dot{m}_{\mathrm{C1C2}} = \dot{m}_{\mathrm{C2C1}} = 0$).

In order to investigate the transient behavior of the process for these two case studies, we ran a series of dynamic simulations with the process model described in section "Process model". It is also necessary to specify the initial conditions in each processing unit. This entails specifying the particle size distributions (PSDs) of the seed crystals of both enantiomers,

as well as the initial composition of the solution in all processing units. The PSDs of the seed crystals in the crystallizers are assumed to follow normal distributions with modal size 100 μm and standard deviation of 20 μm (with the tail of the distribution extending to negative particle sizes cut off). The number of seed particles is adjusted to achieve a certain initial enantiomeric excess and a certain total seed mass. In all simulations presented in this article, we choose to specify the seed PSDs in the mill and the crystallizer on the respective side of the flowsheet to be the same. Furthermore, we specify the initial conditions to be "mirror-symmetric" across the two sides of the flowsheet. To properly specify the enantiomeric purity of the seeds, we define the time-dependent solid state enantiomeric excess in crystallizer i as:

$$\epsilon_{s,\mathrm{C}i}(t) = \frac{\mu^{\mathrm{R}}_{3,\mathrm{C}i}(t) - \mu^{\mathrm{S}}_{3,\mathrm{C}i}(t)}{\mu^{\mathrm{R}}_{3,\mathrm{C}i}(t) + \mu^{\mathrm{S}}_{3,\mathrm{C}i}(t)} \tag{11}$$

Using this definition the specifications on the seed PSDs become:

$$\begin{aligned} &\epsilon_{s,\mathrm{C}1}(0) = -\epsilon_{s,\mathrm{C}2}(0) \\ &\mu^{\mathrm{R}}_{3,\mathrm{C}1}(0) + \mu^{\mathrm{S}}_{3,s,\mathrm{C}1}(0) = \mu^{\mathrm{R}}_{3,\mathrm{C}2}(0) + \mu^{\mathrm{S}}_{3,\mathrm{C}2}(0) \\ &\mu^{j}_{3,\mathrm{M}i}(0) = \mu^{j}_{3,\mathrm{C}i}(0) \end{aligned} \tag{12}$$

The initial composition of the solution in all vessels is taken to be the same as in the feed stream (cf. Table 2), i.e., in this case it is racemic and supersaturated.

Now that we have specified all particulars of case studies 1 and 2, we can investigate the dynamic behavior of the flowsheet in both cases in order to investigate potential steady states and their stability. To this end, we

report the evolution of the solid state enantiomeric excess in crystallizer 1, $\epsilon_{s,\mathrm{C1}}(t)$, starting from initial values of $\epsilon_{s,\mathrm{C1}}(0) = \{1; 0.7; 0.5; 0.33; 0\}$ (from enantiomerically pure seed material to racemic seed material) in Figure 4. Focusing first on case study 1 (Figure 4a), where we specified a substantial solution exchange flow rate between the crystallizers, we see that the solid state enantiomeric excess approaches unity for all cases except for the case where we started in perfectly racemic conditions ($\epsilon_{s,\mathrm{C1}}(0) = 0$, solid blue line). Since the flowsheet is completely symmetric in this case, this indicates that we can obtain the pure desired enantiomer from crystallizer 1 and the pure counter-enantiomer from crystallizer 2. Note that in all cases with an initial solid state enantiomeric excess we first observe a decrease in enantiomeric excess before the system recovers and reaches the pure steady state. This is caused by the selection of the initial solution state. Since it is racemic, but strongly supersaturated, crystals of both enantiomers nucleate initially, which decreases the enantiomeric excess. It is especially noteworthy that under these conditions the flowsheet is able to reject large amounts of enantiomeric impurities that are present in the initial seed material. From this analysis, we can surmise that there must be (at least) two steady states for case study 1: a stable steady state yielding the desired and counter-enantiomer in pure form from the respective crystallizer and an unstable steady state yielding both enantiomers in racemic composition from both crystallizers. This inherently stable behavior stands in stark contrast to any batch process using preferential crystallization. In such batch processes even a slight amount of enantiomeric impurity in the seed material alters the trajectory significantly for the worse; especially when secondary nucleation

kinetics are significant.

Turning our attention now to case study 2 (Figure 4b), where we specified the crystallizers to be decoupled (without solution exchange between them), we see that all trajectories are converging to the racemic steady state, except for the one that already starts at full enantiomeric purity (i.e., $\epsilon_{s,\mathrm{C1}}(0) = 1$, solid black line). Thus, the steady state stability in this case study is exactly reversed from case study 1: the racemic steady state is the stable one, while the enantiopure steady state is the unstable one. Additionally to the process simulations shown in Figure 4b, we have also conducted simulations for much longer times (> 400 hours) with only minor amounts of enantiomeric impurity (< 1 wt% of total seed mass) present in the initial state. Even in these cases, the simulations converged to the racemic steady state. Note that while the steady state behavior is exactly reversed in case studies 1 and 2, the dynamic approach to the respective steady states occurs generally much faster in case study 2 at comparable levels of enantiomeric impurity. From this investigation we conclude that a significant exchange rate between the two crystallizers, which racemizes the composition of the solution phase and therefore reduces the supersaturation of the counter-enantiomer in each crystallizer, is able to stabilize the enantiopure steady state significantly. We consider operating the process in such an inherently stable fashion to be highly beneficial when aiming for enantiopure products via continuous preferential crystallization.

Time to steady state

In the previous section we identified that different seed purities alter the time required to reach the enantiopure steady state in case study 1. It seems evident that also the overall seed mass added to the processing units will influence the time required to reach steady state. In order to further investigate this effect, we now report simulations with varying enantiomeric excess in the feed material and varying total seed mass, while all other conditions are kept as in case study 1. We converged all these process simulations to their enantiopure steady state and report the time to steady state as the last time at which the enantiomeric excess in the solid phase is smaller than 0.99 in crystallizer 1 (and thus greater than -0.99 in crystallizer 2). The resulting data are shown in Figure 5, where the time to steady state (color scale) is reported with respect to the relative seed mass (normalized by the expected yield at steady state) and the enantiomeric excess present in the seed material.

From that figure we can see that a high enantiomeric purity in the seed material yields a much shorter time to steady state. The total seed mass on the other hand does not change the time to steady state signficantly. This is a consequence of how we have defined the time to steady state: we have exclusively focused on the time that is required to obtain an enantiomerically pure solid product from the two crystallizers, while we have chosen to neglect all liquid phase properties in the crystallizers. If massive amounts of seeds are supplied to the crystallizers, the supersaturation in the crystallizers crashes to a low value and only slowly recovers to its steady state

value (something that one might term "over-seeding"). Vice versa, if the seed amount is chosen to be small, the supersaturation in the liquid phase takes longer to sink to the steady state supersaturation, which could be referred to as "under-seeding". However, our definition of the time to steady state does not include such considerations because we are focusing on the enantiomeric purity in the obtained product streams exclusively.

Identification of process parameters that yield enantiopure products

In section "Determination of steady states and their stability" we identified two possible outcomes of steady state stability of the overall flowsheet, which were identified by changing the exchange flow rate between the crystallizers. It would seem logical that the residence time in the crystallizers, which is chiefly affected by the outlet flow rate to the filtration units ($\dot{m}_{\mathrm{C}i\mathrm{F}i}$), will influence the stability of the steady states as well. In order to show this effect, we have carried out additional process simulations varying these flow rates at otherwise identical conditions to case study 1 (cf. Table 2). For this analysis, we have conducted process simulations starting from an initial solid state enantiomeric excess ($\epsilon_{s,\mathrm{C1}}(0) = 0.5$ and $\epsilon_{s,\mathrm{C2}}(0) = -0.5$) and have varied the exchange flow rates ($\dot{m}_{\mathrm{C}i\mathrm{C}p}$) and outlet flow rates from the crystallizers to the filtration units ($\dot{m}_{\mathrm{C}i\mathrm{F}i}$) and subsequently determined the stable steady state for these process configurations. The results are reported in Figure 6a where we indicate the processing conditions that lead to enantiomerically pure products as the green region and the processing conditions that yield a racemic solid state product as the grey region. In

order to create this plot, we ran 400 simulations for a total process time of 50 hours with the relevant flow rates distributed on a linear grid. Note that for some of these flow rate combinations the simulations did not yet converge to either the racemic ($\epsilon_{s,\mathrm{C1}}(t = 50\,\mathrm{h}) \geq 0.01$) or the enantiopure steady state ($\epsilon_{s,\mathrm{C1}}(t = 50\,\mathrm{h}) \leq 0.99$). While there was a clear tendency to which outcome would eventually prevail in these simulations, we refrain from assigning them to either the grey or the green region and report them as the striped region in Figure 6a. By extending these simulations to longer processing times, we could eventually determine their outcome, but we deemed the computational effort for this exercise to be unreasonably high. Furthermore, such process conditions, where the steady state is approached very slowly, are inherently unattractive and should be avoided. Regardless, from Figure 6a we gather that there is a considerable range of processing conditions where an enantiopure product (green region) can indeed be obtained; including processing conditions with reasonable values for all flow rates. Two further points are worth making with respect to the shape of the green region in Figure 6a: first, we could identify that there is a threshold exchange flow rate between the two crystallizers which enables obtaining enantiopure products. However, this threshold occurs at increasingly small residence times of the particles in the crystallizer (large outlet flow rates). One could conjecture that the threshold exchange flow rate might be asymptotically decreased to zero for even larger outlet flow rates. Since this condition is equivalent to a short particle residence time in the crystallizer, these process conditions would involve increasingly massive recycle flow rates for the mother liquor if an acceptable yield were still to be obtained. Hence, such process-

ing conditions are impractical. Second, the exchange flow rate required to obtain an enantiomerically pure product at small outlet flow rates (large particle residence times in the crystallizer) increases rapidly. This indicates that a similarly impractical behavior for long particle residence times exists as well, i.e., for these long particle residence times an increasingly large exchange flow rate is needed to stabilize the process sufficiently.

In order to investigate the effect of further processing conditions, we also varied the temperature and size of the suspension mills, as reported in Figures 6b to 6f. Raising the temperature in the suspension mills affects the process by providing a higher driving force for the dissolution of fine particles and increasing the size of the mills increases the residence time in the mills (therefore allowing more time for particles to get milled and more time for nuclei to dissolve). Both of these effects should impact the stability of the process positively, however, these changes also negatively impact the productivity of the process (if the recycle/purge ratio for the mother liquor is kept constant). Indeed, in the above-mentioned additional subfigures of Figure 6, we see that the green region, where enantiomerically pure products can be obtained, changes its position in the exchange flow rate vs. outlet flow rate plane. However, it is noteworthy that the same general behavior for the shape of the green region is observed, therefore further substantiating the observations made before. Further analyzing the data shown in these figures, we see that an increase in the suspension mill temperature shifts the green region towards lower outlet flow rates and lower exchange flow rates (lower left of the plane), which indicates that a wider range of realistic flow rates allows obtaining enantiomerically pure products. An increase in

the mill's size (increase in residence time in the mill) on the other hand shifts the green region towards lower exchange flow rates, but higher outlet flow rates (bottom right corner of the plane). This indicates that providing the additional residence time in the mill at temperatures higher than in the crystallizer might help with the dissolution of undesired nuclei of the counter-enantiomer, but it also allows more time for small particles of the desired enantiomer to dissolve, which at the same time are produced in greater numbers because there is also more time for particle breakage in the mill.

Investigation of enriched feed streams

In the cases discussed so far we have always supplied a racemic feed stream to the processing flowsheet and showed that enantiopure products can be obtained from such streams in a wide range of processing conditions. However, the feed stream supplied to a crystallization process might already have undergone some kind of enrichment in the desired enantiomer (e.g., by asymmetric synthesis or another separation process). Therefore, it seems prudent to investigate the performance of our continuous preferential crystallization flowsheet for these cases as well. Hence, we introduce process simulations with enriched feed streams with compositions that still lie within the three phase region of the ternary phase diagram at a given temperature. At this point it is noteworthy that such an enantiomerically enriched composition can always be shifted into the two phase region for a conglomerate by either increasing the temperature or removing solvent selectively (e.g., by distillation). To illustrate this in Figure 7, we have drawn the case where we have

increased the temperature (red phase boundaries) for a batch vessel in such a way that the initial feed composition (green circle) lies at the border of the two phase region. In this case the optimal yield of a batch crystallizer operated in such a fashion is indicated by the orange square in the diagram. Note that this is the only thermodynamically stable fashion to operate a batch crystallizer that guarantees obtaining an enantiomerically pure product (barring any non-idealities, such as inclusions of the counter-enantiomer in the crystals). Solvent removal by distillation on the other hand might not be desirable due to potential thermal degradation of the product or simply because of the additional energy requirements that such a process entails.

In contrast, the continuous preferential crystallization process can be operated in a stable fashion in the three phase region of the diagram (as already shown for racemic feed streams above) and is thus allowed to operate at a lower temperature (blue phase boundaries). Ideally, the continuous process would therefore be able to reach the steady state condition at the grey triangle (which is just barely supersaturated at the lower temperature), i.e., potentially leading to a higher yield.

Operating the continuous preferential crystallization flowsheet in Figure 3 with enantiomerically enriched feed streams entails altering the way the crystallizers are fed. Specifically, introducing the enriched feed stream exclusively into the crystallizer producing crystals of the enantiomer in which the feed stream is already enriched is preferable (so that no feed stream enters the second crystallizer, i.e., $\dot{m}_{\mathrm{SC2}} = 0$). The second crystallizer producing the crystals of the counter-enantiomer is then fed by an increased exchange flow rate from the first crystallizer, i.e., we specify $\dot{m}_{\mathrm{C1C2}} > \dot{m}_{\mathrm{C2C1}}$. Conse-

quently, since a lower amount of counter-enantiomer needs to be removed, the processing units that produce crystals of the counter-enantiomer can be scaled down. In the following we will scale down the size of the processing units involved in the production of the counter-enantiomer crystals with a scaling factor s defined as:

$$s = \frac{m_{\mathrm{C2}}}{m_{\mathrm{C1}}} \tag{13}$$

We will further use the same scaling factor to scale the flow rates on that side of the flowsheet. For the outlet flow rate from the primary crystallizer to its filtration unit and the exchange flow rate between the crystallizers, we would like to select values that lie within the green region determined for the racemic feed streams (cf. Figure 6). However, at low values of s (i.e., a small crystallizer for the counter-enantiomer producing side), it becomes unrealistic to draw significant liquid streams from it (even though it becomes replaced by an appropriate incoming stream), as this would result in unrealistic short liquid phase residence times in the small crystallizer. Consequently, we decided to scale the exchange flow rates between the crystallizers with the scaling factor as well. An overview of processing parameters for the simulations using the enriched feed streams resulting from these considerations is reported in Table 3.

Towards a scaling law for the process

In the following, we investigate the steady state outcome of the continuous crystallization flowsheet for different feed enantiomeric excesses and different scaling factors using the scaled process streams and sizes of processing vessels

reported in Table 3. For this purpose, the feed enantiomeric excess, ϵ_f, is defined as

$$\epsilon_f = \frac{w^{\mathrm{R}}_{\mathrm{SC1}} - w^{\mathrm{S}}_{\mathrm{SC1}}}{w^{\mathrm{R}}_{\mathrm{SC1}} + w^{\mathrm{S}}_{\mathrm{SC1}}} \tag{14}$$

In Figure 8 we report the solid state enantiomeric excess at steady state obtained in the main crystallizer (C1) vs. the scaling factor s for feed streams with different enantiomeric excesses, ϵ_f. Focusing first on the case with a modestly enriched feed stream ($\epsilon_f = 0.125$; blue triangles) we see that an enantiomerically pure product can only be obtained with scaling factors near unity, i.e., the processing units producing the counter-enantiomer are required to be of almost equal size to the processing units producing the desired enantiomer. Further downscaling of the processing units on the r.h.s. in the flowsheet leads to a drop in solid state enantiomeric excess obtained at the steady state. Note that we only report the solid state enantiomeric excess at the steady state for the larger crystallizer in Figure 8, however, the smaller crystallizer reached enantiomeric purity as well (with respect to the counter enantiomer, i.e., $\epsilon_{s,\mathrm{C2}}(t_{\mathrm{ss}}) \leq -0.99$). Additionally, we report the solid state enantiomeric excess that would be obtained from a batch crystallizer reaching the thermodynamic equilibrium as the dashed lines in that figure. The continuous process on the other hand does *not* reach the thermodynamic equilibrium, i.e., the steady state is slightly supersaturated for both enantiomers. This leads to higher solid state enantiomeric excess in the continuous process even when the processing units on the counter-enantiomer side of the flowsheet are scaled down beyond the minimum scaling factor that guarantees enantiomerically pure solids. Focusing now on the addi-

tional lines at higher feed enantiomeric excesses ($\epsilon_f = \{0.250; 0.375; 0.500\}$; red green and black symbols, respectively), we see that the minimum scaling factor leading to enantiomerically pure solids decreases with increasing feed enantiomeric excess, as one might have expected.

Performing this investigation for additional values of the feed enantiomeric excess, we can obtain a series of minimum scaling factors, $s_{\min}$. We report these minimum scaling factors extracted from this extended series of simulations as the data points in Figure 9. These data points can be well described by a second order polynomial, which is reported in the same figure. This polynomial can be used as an empirical scaling rule for the process flowsheet to decide the minimum size of the processing vessels for the counter-enantiomer side of the flowsheet, which still guarantees enantiomerically pure products. Note that this scaling rule is only valid for the crystallization and breakage kinetics listed in Table 1 and the processing and scaling conditions reported in Table 3. Altering these parameters or the kinetics will result in a modified scaling law as well.

Comparison with batch crystallization

The viability of the new continuous process flowsheet in Figure 3 is clear for racemic feed streams for a conglomerate forming system of enantiomers since a batch process cannot reach enantiomeric purity in that case, i.e., in its thermodynamic equilibrium the batch process will always yield equal amounts of both enantiomers (apart from any seed material that is introduced) when starting from a racemic initial point. However, as detailed previously (cf. Figure 7), the application of the designed continuous flowsheets

to enantiomerically enriched feed streams needs to be justified, because a crystallization process carried out in a batch can always be shifted to the two phase region of the ternary phase diagram by increasing the temperature. This begs the question: In which cases is running the continuous preferential crystallization flowsheet beneficial for enantiomerically enriched feed streams? To give an answer to this question, we will define the efficiency of the overall continuous process as:

$$\eta_{\text{continuous}} = \frac{k_v \rho_c \mu_{3,\text{C1}}^{\text{R}}(t_{ss})}{m_{\text{C1}} + m_{\text{M1}} + m_{\text{C2}} + m_{\text{M2}}} \tag{15}$$

That is, we define the efficiency $\eta_{\text{continuous}}$ as the mass of desired enantiomer obtained in crystallizer 1 at steady state divided by the mass of suspension in all processing vessels in the flowsheet. The efficiency defined in this way is a proxy for the mass of solvent needed to obtain a given mass of the desired enantiomer in enantiopure form. Similarly, we can define the efficiency of an ideal batch process (as defined above) as:

$$\eta_{\text{batch}} = \frac{k_v \rho_c \mu_{3,\text{batch}}^{\text{R}}}{m_{\text{batch}}} \tag{16}$$

which can be calculated assuming that a batch operated just inside the two phase region eventually reaches the thermodynamic equilibrium. Using the scaling rule presented in the previous section, we can determine the efficiency for the continuous flowsheet at various enantiomeric excesses and likewise for the batch by determining the temperature rise required to reach the two phase region of the phase diagram (which is concomitant

with a yield loss). We report the resulting efficiencies in Figure 10. One can see that the continuous flowsheet outperforms the batch process at low to moderate enantiomeric excesses in the flowsheet (up to $\epsilon_f \approx 0.35$). For higher enantiomeric excesses an ideal batch process is the more efficient processing variant. Note that the efficiency curves should not be extrapolated to racemic feed streams/initial conditions ($\epsilon_f = 0$), as the thermodynamically stable operation of a batch crystallization process becomes infeasible for a racemic starting condition, i.e., the continuous preferential crystallization process outperforms batch crystallization processes by definition at this point. While the results shown in Figure 10 suggest a potentially higher efficiency for the continuous preferential crystallization process presented in this article when compared to an ideal batch crystallization process, the continuous process also comes at the expense of an increased operational complexity. Obviously, this added complexity needs to be carefully balanced with the gain in efficiency together with the gain in productivity due to steady continuous production of the desired enantiomer.

Practical considerations and alternatives

At this point we would like to point out some practical considerations with respect to an experimental implementation of the proposed continuous flowsheet and present some additional alternatives. First, the proposed flowsheet requires pumping suspensions, which can be challenging when a substantial residence time is required in the crystallizer and the mill. For a laboratory scale or low tonnage production scale implementation, the challenge stems from the associated small volumetric flow rates. In wide pipes this would

lead to a small flow velocity, which could lead to the settling of particles in the pipes (and eventual blockages). Narrower pipes with higher flow velocities would, however, also likely be subject to clogging, as the diameter to particle size ratio becomes too small. However, this problem can be circumvented without severe consequences on the "steady state" behavior by using intermittent flow[35,36]. Second, piping, where undesired nucleation or dissolution could occur, would need to be appropriately insulated or temperature controlled. On a laboratory scale this could be accomplished by a tube-in-tube configuration, as for example demonstrated by Galan et al.[25]. Third, it is noteworthy that there exist several alternatives to our proposal using heated mills and filtered exchange streams between the crystallizers. Instead of generating new particles by breaking existing ones in a mill, one could also use an ultrasound source in the crystallizer to induce crystal fragmentation[37]. One could also imagine to promote secondary nucleation of the desired enantiomer. However, the dissolution of undesired nuclei of the counter-enantiomer would still need to be accomplished to achieve the process stability observed in the implementation presented in this manuscript. This could, for example, be accomplished by a heated fines dissolution loop. Instead of using filtered exchange streams between the crystallizers, one could rely on sequestration based on the hydrodynamics of the crystallizer; a strategy that has recently been realized for Grignard reactions in continuous stirred tank reactors.[38]

Concluding Remarks

In this article we have presented a novel continuous preferential crystallization process using two crystallizers that are coupled by exchanging their clear liquid phases with each other. Furthermore, the flowsheet involves the in-situ generation of seed particles using suspension mills (or an equivalent device), which concomittantly may act as fines dissolution units. We have shown that this flowsheet leads to enantiomerically pure products in both crystallizers and that it can be operated in an inherently stable fashion, i.e., an enantiomerically pure steady state can be obtained even from impure initial states. This suggests that the presented process is self-regulating because it will also recover from the sudden appearance of undesired "seeds" of the counter-enantiomer in the crystallizers, which is a phenomenon encountered from time to time in industrial crystallizers due to scale formation at the crystallizer walls. The presented process can therefore be considered to be inherently stable if the processing parameters are correctly chosen. To this end, we have further identified parameter regions that allow obtaining the desired enantiomer in pure form.

While these findings are clearly dependent on the particulars of the specific case study (e.g., the crystallization and breakage kinetics), the presented flowsheet is highly adaptable and should allow overcoming adverse kinetics by tuning the milling intensity, temperatures, etc. While tuning the many degrees of freedom in the flowsheet blindly in experimental studies is clearly ill advised, the process model presented in this article may be used as a tool to understand how the process might react to changes in these param-

eters, therefore enabling a proper design and deeper understanding of the underlying process.

For the case of enriched feed streams we revealed a scaling law for the process and have shown that the continuous process outperforms a batch crystallization process (operated in a thermodynamically stable fashion in the two phase region of the phase diagram) in terms of solvent consumption per mass of enantiopure product. However, this finding is only true in a limited range of feed enantiomeric excesses and comes at the expense of a higher operational complexity. Nonetheless, unveiling and appreciating these tradeoffs enables an informed decision, which is desirable *per se*.

Acknowledgements

This work was supported in part by a Lilly Innovation Fellowship Award to TV from Eli Lilly and Company.

Notation

c	concentration (mass solute per mass of solvent)	[kg kg^{-1}]
$c_\star$	solubility (mass solute per mass of solvent)	[kg kg^{-1}]
d	daughter distribution	[m^{-1}]
D	dissolution rate	[m s^{-1}]
G	crystal growth rate	[m s^{-1}]
J	nucleation rate (per mass of clear liquid)	[kg^{-1} s^{-1}]
k	kinetic/thermodynamic parameters	[varies]

K	breakage rate	[s^{-1}]
L	crystal size	[m]
m	suspension mass	[kg]
n	number density distribution (per mass of suspension)	[kg^{-1} m^{-1}]
$\dot{m}$	mass flow rate	[kg s^{-1}]
s	scaling factor	[-]
S	supersaturation	[-]
t	time	[s]
T	temperature	[K]
w	weight fraction	[-]
ϵ	enantiomeric excess	[-]
η	efficiency	[-]
λ	size of parent particle	[m]
μ_3	third moment of PSD	[m^3 kg^{-1}]
ρ_c	crystal density	[kg m^{-3}]

Superscripts

j	enantiomer
p	counter-enantiomer

Subscripts

Ci	i^{th} crystallizer

f	feed
Fi	i^{th} filtration unit
Mi	i^{th} milling unit
min	minimum
O	outlet (solids)
prim	primary
P	purge (clear liquid)
q	processing unit on opposite flowsheet side
rac	racemic
s	solid state
S	source (feed vessel)
sec	secondary
ss	steady state

References

1. Rajendran A, Paredes G, Mazzotti M. Simulated moving bed chromatography for the separation of enantiomers. *J Chrom A*. 2009; 1216:709–738.

2. Schmidt-Traub H, Schulte M, Seidel-Morgenstern A. *Preparative Chromatography*. Weinheim: Wiley-VCH, 2012.

3. Rekoske J. Chiral Separations. *AIChE J*. 2001;47:2–5.

4. Jacques J, Collet A, Wilen SH. *Enantiomers, Racemates and Resolutions*. Hoboken: Wiley-Blackwell, 1981.

5. Lorenz H, Seidel-Morgenstern A. Processes To Separate Enantiomers. *Angew Chem Int Ed.* 2014;53:1218–1250.

6. Wilen S, Collet A, Jacques J. Strategies in optical resolution. *Tetrahedron.* 1977;33:2725–2736.

7. Marchand P, Lefèbre L, Querniard F, Cardinaël P, Perez G, Counioux JJ, Coquerel G. Diastereomeric resolution rationalized by phase diagrams under the actual conditions of the experimental process. *Tetrahedron Asymmetry.* 2004;16:2455–2465.

8. Faigl F, Fogassy E, Nógrádi M, Pálovics E, Schindler J. Strategies in optical resolution: a practical guide. *Tetrahedron Asymmetry.* 2008; 19:519–536.

9. Schroer J, Wibowo C, Ng K. Synthesis of chiral crystallization processes. *AIChE J.* 2001;47:369–387.

10. Coquerel G. Crystallization of molecular systems from solution: phase diagrams, supersaturation and other basic concepts. *Chem Soc Rev.* 2014;42:2286–2300.

11. Temmel E, Wloch S, Müller U, Grawe D, Eilers R, Lorenz H, Seidel-Morgenstern A. Separation of systems forming solid solutions using counter-current crystallization. *Chem Eng Sci.* 2013;104:662–673.

12. Davey R, Sadiq G, Back K, Wilkinson L, Seaton C. The isolation of a metastable conglomerate using a combined computational and controlled crystallization approach. *Chem Commun.* 2012;48:1976–1978.

790 13. Wermester N, Aubin E, Pauchet M, Coste S, Coquerel G. Preferential
791 crystallization in an unusual case of conglomerate with partial solid
792 solutions. *Tetrahedron Asymmetry.* 2007;18:821–831.

793 14. Codan L, Casillo S, Bäbler M, Mazzotti M. Phase Diagram of a Chi-
794 ral Substance Exhibiting Oiling Out. 2. Racemic Compound Forming
795 Ibuprofen in Water. *Cryst Growth Des.* 2012;12:5298–5310.

796 15. Tamura R, Fujimoto D, Lepp Z, Misaki K, Miura H, Takahashi H, Ushio
797 T, Nakai T, Hirotsu K. Mechanism of Preferential Enrichment, an Un-
798 usual Enantiomeric Resolution Phenomenon Caused by Polymorphic
799 Transition during Crystallization of Mixed Crystals Composed of Two
800 Enantiomers. *J Am Chem Soc.* 2002;124:13139–13153.

801 16. Coquerel G. *Preferential Crystallization in Novel Optical Resolution*
802 *Technologies.* Heidelberg, Germany: Springer, 2007.

803 17. Viedma C. Chiral Symmetry Breaking During Crystallization: Com-
804 plete Chiral Purity Induced by Nonlinear Autocatalysis and Recycling.
805 *Phys Rev Lett.* 2005;94:065504.

806 18. Norduuin W, Izumi K, Millemaggi A, Leeman M, Meekes H, Van Enck-
807 evort W, Kellogg R, Kaptein B, Vlieg E, Blackmond D. Emergence of a
808 Single Solid Chiral State from a Nearly Racemic Amino Acid Derivative.
809 *J Am Chem Soc.* 2008;130:1158–1159.

810 19. McBride J, Tully J. Did Life Grind to a Start? *Nature.* 2008;452:161–
811 162.

20. Iggland M, Mazzotti M. A Population Balance Model for Chiral Resolution via Viedma Ripening. *Cryst Growth Des.* 2011;11:4611–4622.

21. Levilain G, Coquerel G. Pitfalls and rewards of preferential crystallization. *CrystEngComm.* 2010;12:1983–1992.

22. Levilain G, Eicke M, Seidel-Morgenstern A. Efficient Resolution of Enantiomers by Coupling Preferential Crystallization and Dissolution. Part 1: Experimental Proof of Principle. *Cryst Growth Des.* 2012; 12:5396–5401.

23. Qamar S, Elsner M, Hussain I, Seidel-Morgenstern A. Seeding strategies and residence time characteristics of continuous preferential crystallization. *Chem Eng Sci.* 2011;71:5–17.

24. Qamar S, Galan K, Elsner M, Seidel-Morgenstern A. Theoretical investigation of simultaneous continuous preferential crystallization in a coupled mode. *Chem Eng Sci.* 2013;98:25–39.

25. Galan K, Eicke M, Elsner M, Lorenz H, Seidel-Morgenstern A. Continuous Preferential Crystallization of Chiral Molecules in Single and Coupled Mixed-Suspension Mixed-Product-Removal Crystallizers. *Cryst Growth Des.* 2015;15:1808–1818.

26. Elsner M, Ziomek G, Seidel-Morgenstern A. Efficient separation of enantiomers by preferential crystallization in two coupled vessels. *AIChE J.* 2009;55:649–649.

27. Elsner M, Ziomek G, Seidel-Morgenstern A. Simultaneous preferential

crystallization in a coupled batch operation mode. Part II: Experimental study and model refinement. *Chem Eng Sci.* 2011;66:1269–1284.

28. Chaaban J, Dam-Johansen K, Skovby T, Kiil S. Separation of Enantiomers by Continuous Preferential Crystallization: Experimental Realization Using a Coupled Crystallizer Configuration. *Org Process Res Dev.* 2013;17:1010–1020.

29. Chaaban J, Dam-Johansen K, Kiil S, Skovby T. Separation of Enantiomers by Continuous Preferential Crystallization: Mathematical Modeling of a Coupled Crystallizer Configuration. *Org Process Res Dev.* 2014;18:601–612.

30. Randolph AD, Larson MA. *Theory of Particulate Process: Analysis and Techniques of Continuous Crystallization.* New York: Academic Press, 2nd edition, 1988.

31. Ramkrishna D. *Population Balances: Theory and Applications to Particulate Systems in Engineering.* San Diego: Academic Press, 2000.

32. Gunawan R, Fusman I, Braatz R. High resolution algorithms for multidimensional population balance equations. *AIChE J.* 2004;50:2738–2749.

33. MATLAB. *version 8.4 (R2014b).* Natick, Massachusetts: The MathWorks Inc., 2014.

34. Sapoundjiev D, Lorenz H, Seidel-Morgenstern A. Solubility of Chiral Threonine Species in Water/Ethanol Mixtures. *J Chem Eng Data.* 2006; 51:1562–1566.

35. Quon J, Zhang H, Alvarez A, Evans J, Myerson A, Trout B. Continuous Crystallization of Aliskiren Hemifumarate. *Cryst Growth Des.* 2012; 12:3036–3044.

36. Powell K, Saleemi A, Rielly C, Nagy Z. Periodic steady-state flow crystallization of a pharmaceutical drug using MSMPR operation. *Chem Eng Proc.* in press;page doi:10.1016/j.cep.2015.01.002.

37. Kim S, Wei C, Kiang S. Crystallization process development of an active pharmaceutical ingredient and particle engineering via the use of ultrasonics and temperature cycling. *Org Process Res Dev.* 2003; 7:997–1001.

38. Wong S, Changi S, Shields R, Bell W, McGarvey B. Operation Strategy Development for Grignard Reaction in a Continuous Stirred Tank Reactor. *Proceedings of the 2014 AIChE Annual Meeting.* 2014;.

List of Figures

Figure 4: Transient behavior of the solid state enantiomeric excess in crystallizer 1 for two case studies (as specified in Table 2): (a) case study 1 (with solution exchange between crystallizers), (b) case study 2 (decoupled crystallizers). The different lines correspond to simulations starting from different initial solid state enantiomeric excesses (different purity of seed particles), i.e., $\epsilon_{s,\mathrm{C1}}(0) = \{1; 0.7; 0.5; 0.33; 0\}$ for the black solid, magenta dash dotted, green dotted, red dashed and blue solid lines, respectively. Note that the time scale in the two figures is different.

Figure 5: Time to steady state for varying total seed amounts and varying enantiomeric purity of the seed material. All other parameters are kept as in case study 1, cf. Table 2. Note that the total seed mass has been normalized with respect to the expected yield at steady state and is plotted on a logarithmic scale.

Figure 6: Parameter study to identify regions where enantiopure products can be obtained when varying exchange flow rate between crystallizers and outlet flow rate from crystallizer to filtration unit. Green regions refer to processing conditions where enantiopure products are obtained; grey regions refer to racemic products; striped regions refer to cases where the eventual steady state was not reached within the total process simulation time of 50 hours. The size and temperature of the suspension mills is varied from subfigure to subfigure.

Figure 7: Qualitative ternary phase diagram of a conglomerate forming system with an ideal batch and a continuous process drawn into it. The solid blue lines are phase boundaries at a low temperature, the dashed red lines are phase boundaries at a high temperature. The symbols indicate the initial/feed point of the process (green circle), the ideal operating point of the continuous process operated at the lower temperature (grey triangle) and the ideal final point of a batch crystallization process operated in the two phase region at the higher temperature (orange square).

List of Tables

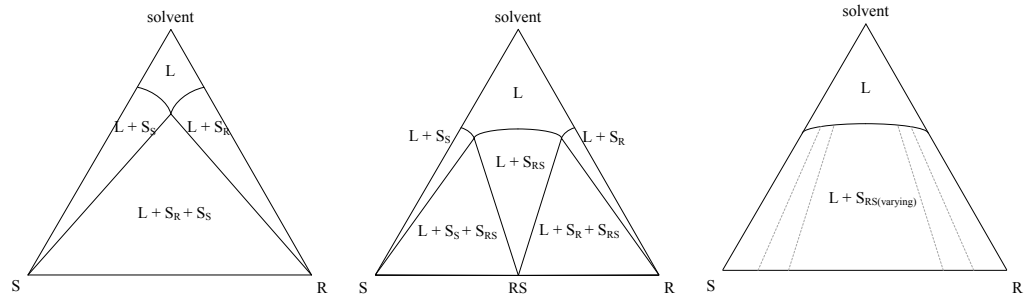

Figure 1: Qualitative ternary phase diagrams of systems of enantiomers: (a) Conglomerate forming system with two 2 phase regions and one 3 phase region, (b) Racemic compound forming system with three 2 phase regions and two 3 phase regions, and (c) solid solution forming system with one 2 phase region.

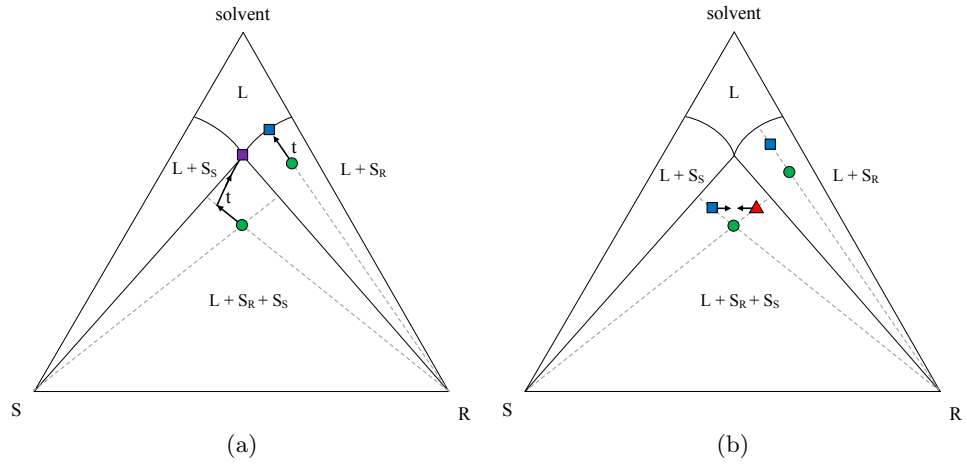

Figure 2: Process variants for a conglomerate forming system depicted in qualitative ternary phase diagrams: (a) batch crystallization processes, (b) continuous crystallization processes. The grey dashed lines in the two phase regions are tie lines, while they are material balance lines in the three phase regions. The green circles are initial (batch) and feed (continuous) points, the squares and triangles are final (batch) and operating (continuous) points.

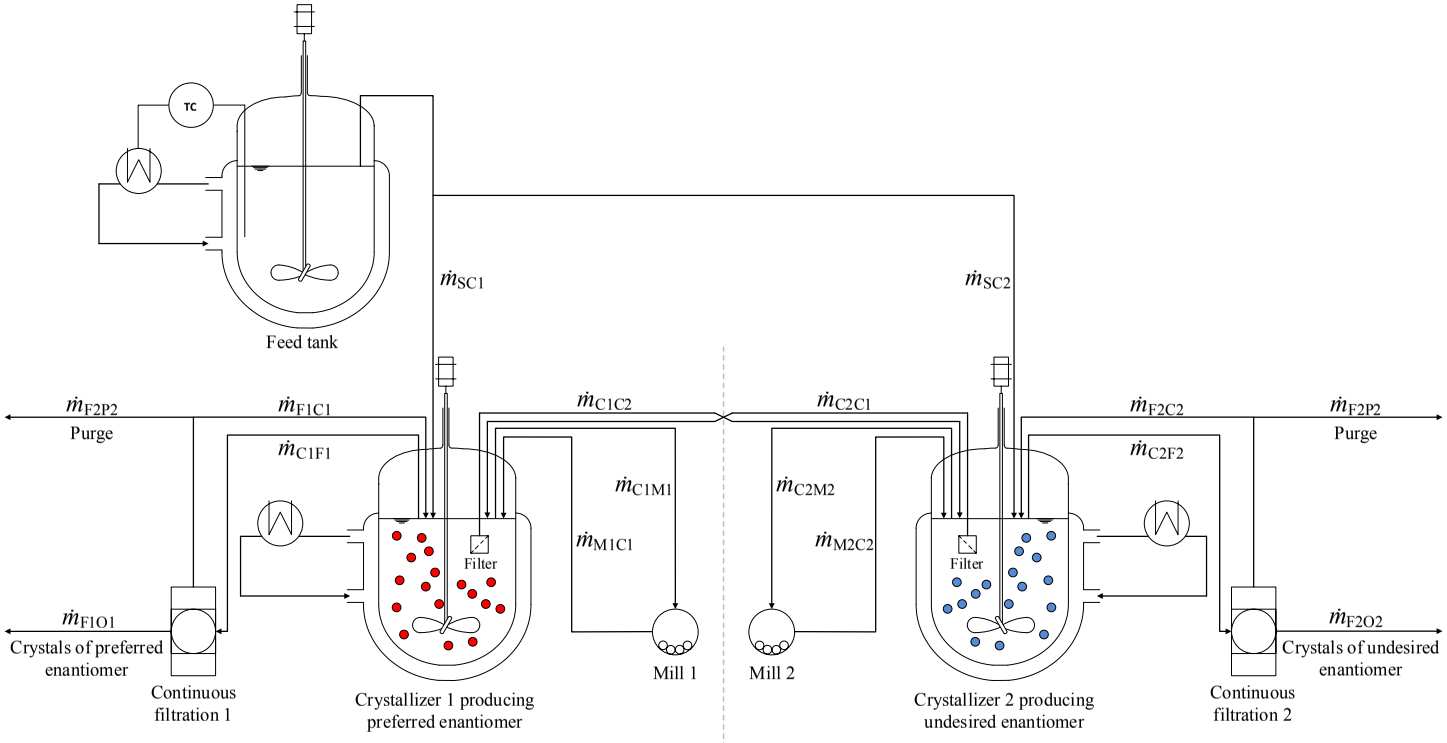

Figure 3: Process flowsheet used in this work consisting of two continuous crystallizers whose liquid phases are exchanged. Suspension mills are connected in a loop to the crystallizers to generate a sufficient amount of seeds in-situ. Note that the mills can be operated at an elevated temperature (with respect to the crystallizer) in order to dissolve fines of the undesired enantiomer generated by nucleation.

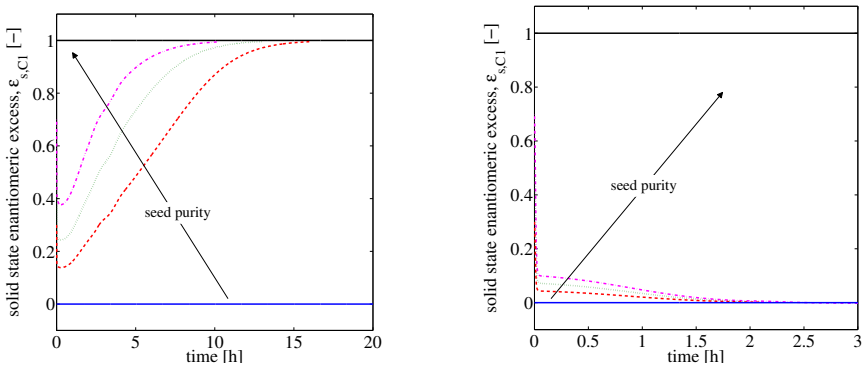

Figure 4: Transient behavior of the solid state enantiomeric excess in crystallizer 1 for two case studies (as specified in Table 2): (a) case study 1 (with solution exchange between crystallizers), (b) case study 2 (decoupled crystallizers). The different lines correspond to simulations starting from different initial solid state enantiomeric excesses (different purity of seed particles), i.e., $\epsilon_{s,\mathrm{C1}}(0) = \{1; 0.7; 0.5; 0.33; 0\}$ for the black solid, magenta dash dotted, green dotted, red dashed and blue solid lines, respectively. Note that the time scale in the two figures is different.

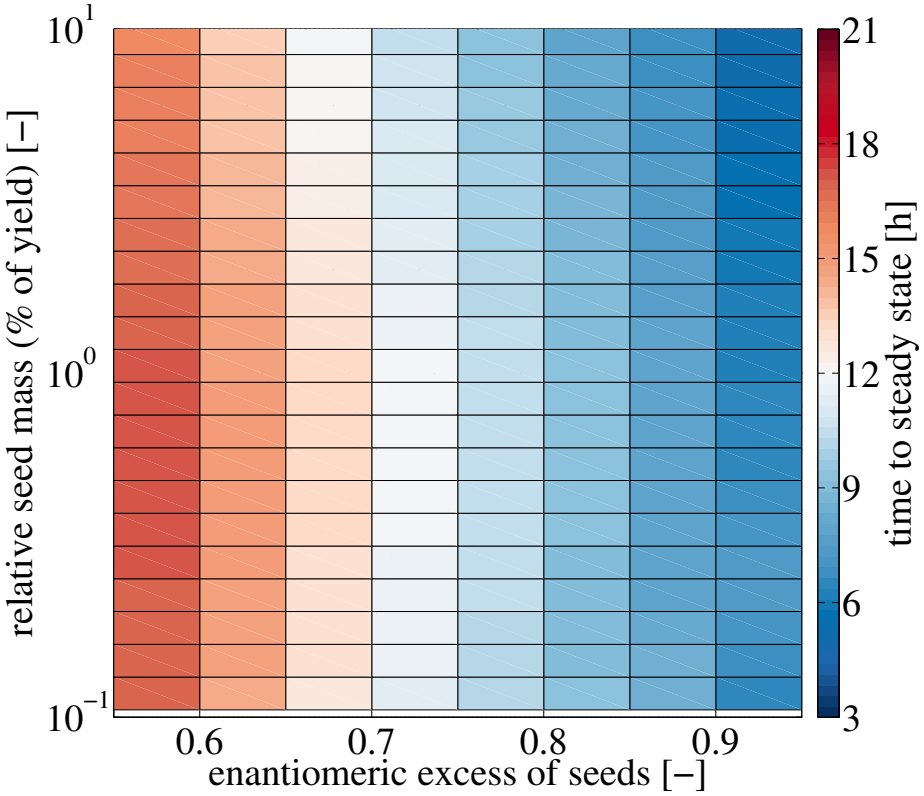

Figure 5: Time to steady state for varying total seed amounts and varying enantiomeric purity of the seed material. All other parameters are kept as in case study 1, cf. Table 2. Note that the total seed mass has been normalized with respect to the expected yield at steady state and is plotted on a logarithmic scale.

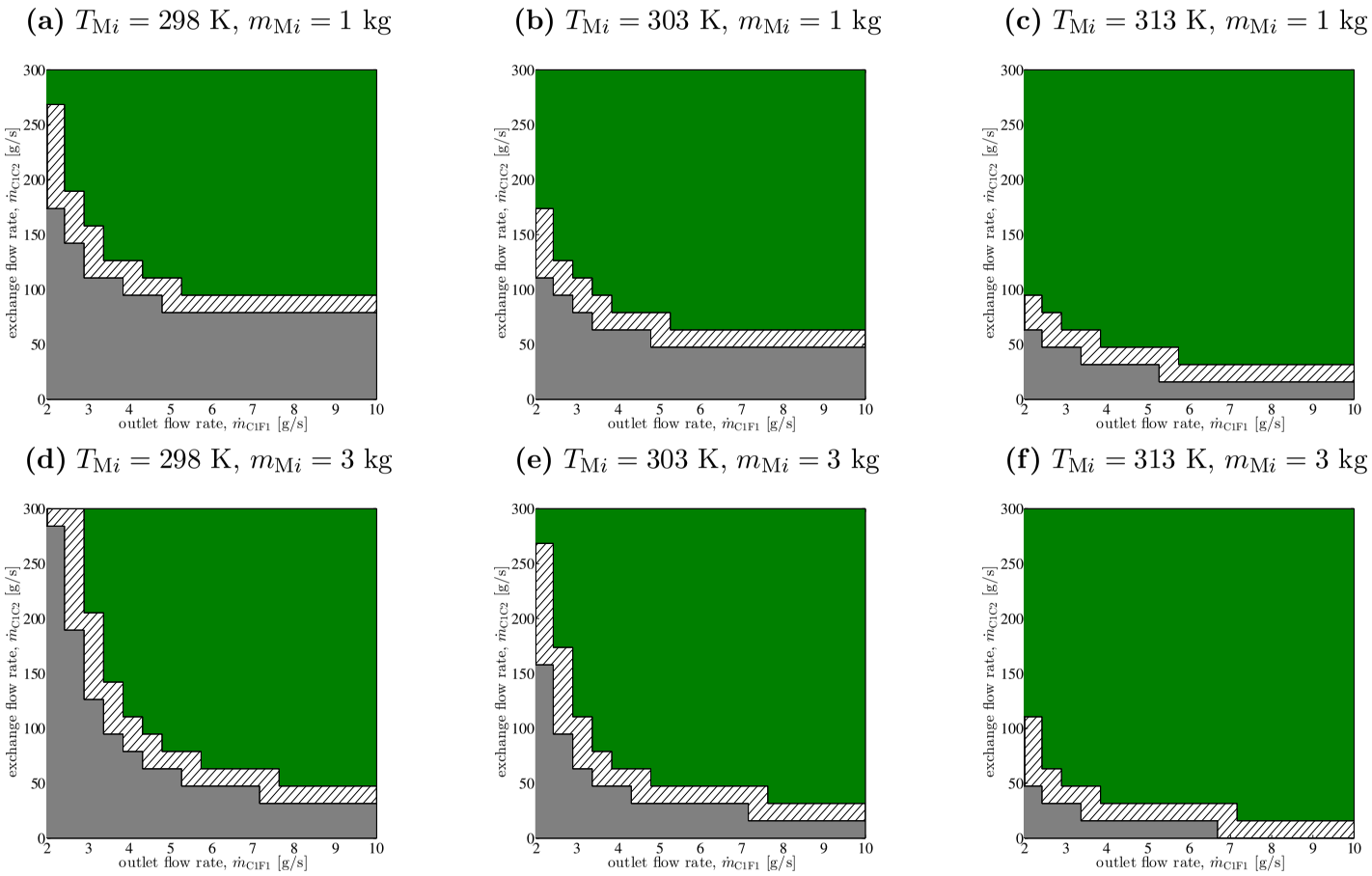

Figure 6: Parameter study to identify regions where enantiopure products can be obtained when varying exchange flow rate between crystallizers and outlet flow rate from crystallizer to filtration unit. Green regions refer to processing conditions where enantiopure products are obtained; grey regions refer to racemic products; striped regions refer to cases where the eventual steady state was not reached within the total process simulation time of 50 hours. The size and temperature of the suspension mills is varied from subfigure to subfigure.

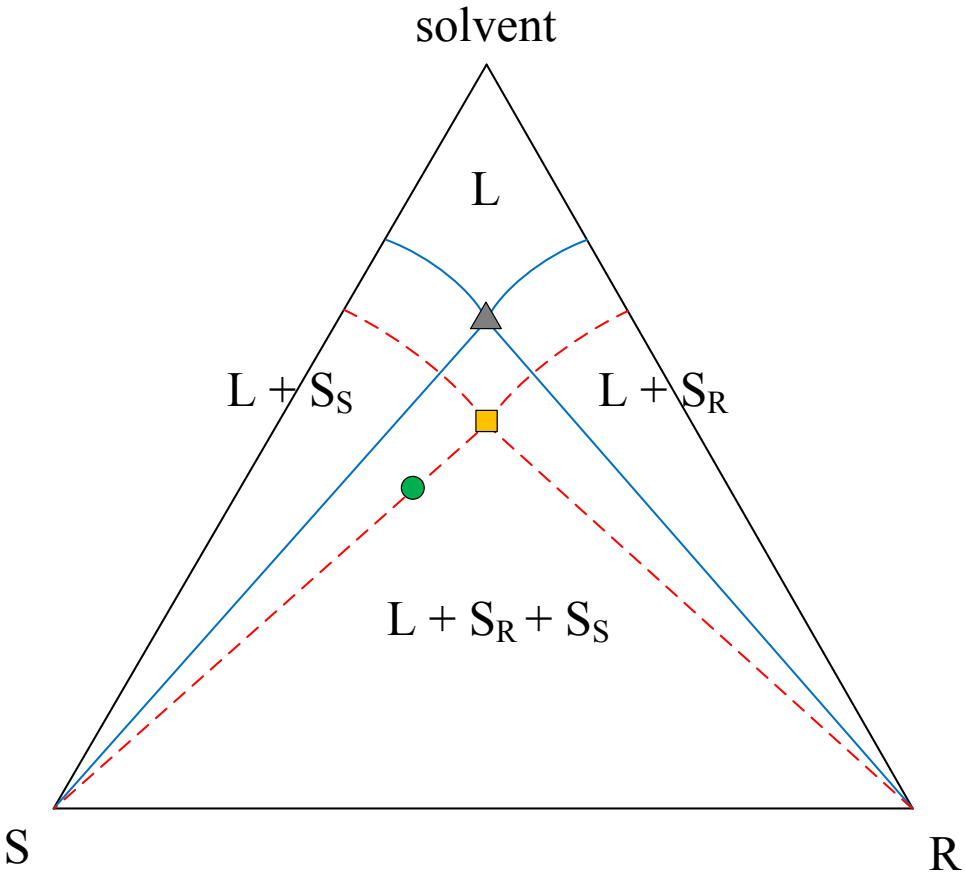

Figure 7: Qualitative ternary phase diagram of a conglomerate forming system with an ideal batch and a continuous process drawn into it. The solid blue lines are phase boundaries at a low temperature, the dashed red lines are phase boundaries at a high temperature. The symbols indicate the initial/feed point of the process (green circle), the ideal operating point of the continuous process operated at the lower temperature (grey triangle) and the ideal final point of a batch crystallization process operated in the two phase region at the higher temperature (orange square).

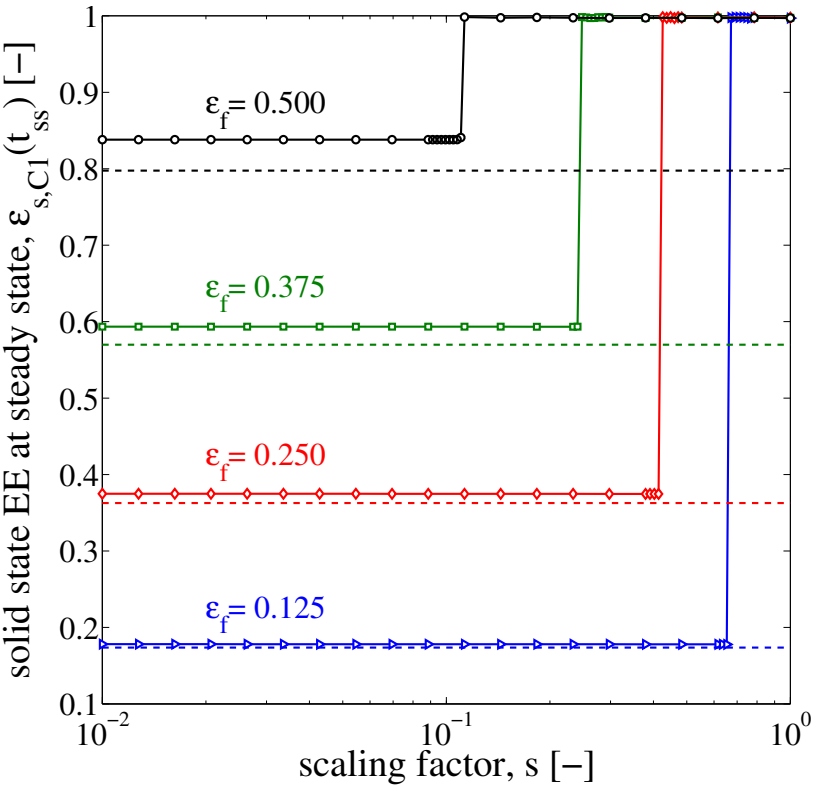

Figure 8: Solid state enantiomeric excess obtained in crystallizer 1 at steady state for different feed enantiomeric excesses vs.scaling factor. Symbols: data points obtained from the simulations; solid lines are merely a guide to the eye. The dashed lines represent the enantiomeric excess of the solid phase in the thermodynamic equilibrium. Note the logarithmic scale for the scaling factor s.

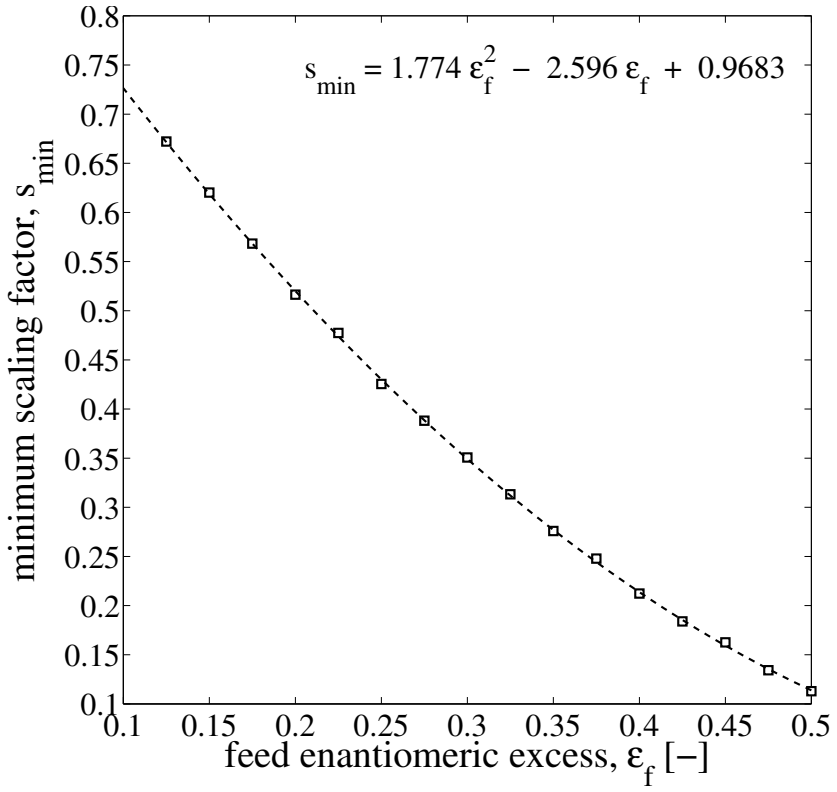

Figure 9: Minimum scaling factor that still yields enantiomerically pure solids vs. feed enantiomeric excess. Square symbols represent simulation results; the dashed line is a second order polynomial fitted to the datapoints.

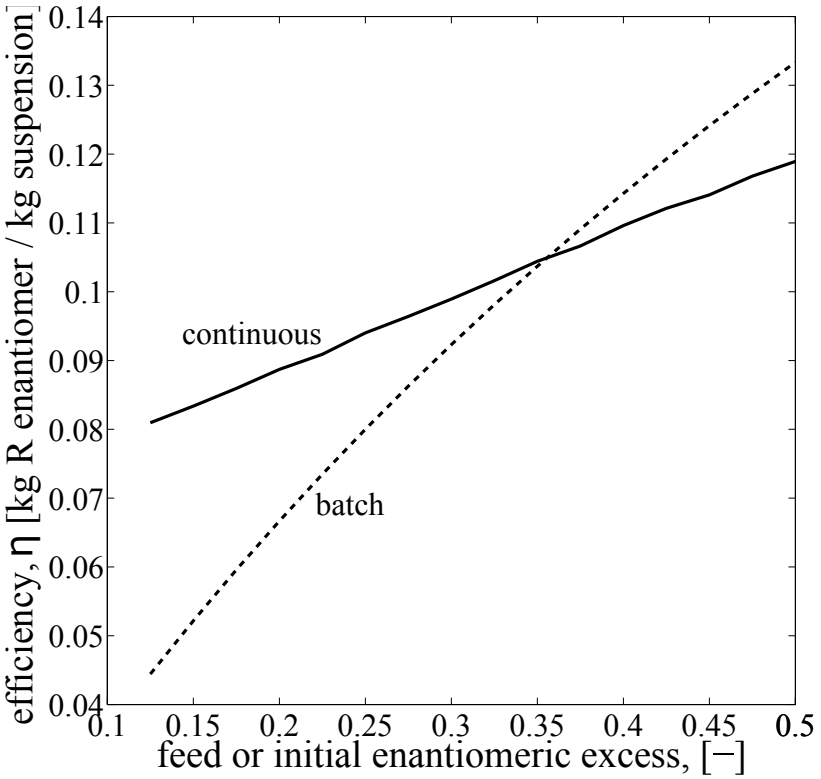

Figure 10: Efficiency (cf. Eqs. (15) and (16)) per suspension mass for a batch crystallizer operating in the two phase region and the continuous preferential crystallization flowsheet in dependence of the feed/initial enantiomeric excess.

Table 1: Substance data used in the threonine case study[a]

solubility [b]	$c_{\star,\mathrm{rac}} = k_{\mathrm{c1}} + k_{\mathrm{c2}}T + k_{\mathrm{c3}}T^2$
	k_{c1} 5.139×10^{-1}
	k_{c2} 3.848×10^{-3} K^{-1}
	k_{c3} 8.067×10^{-6} K^{-2}
crystal growth[c]	$G = k_{\mathrm{g1}} \exp\left(-\frac{k_{\mathrm{g2}}}{T}\right) (S-1)^{k_{\mathrm{g3}}} (1 + k_{\mathrm{g4}}L)^{k_{\mathrm{g5}}}$
	k_{g1} 4.968×10^{7} m s^{-1}
	k_{g2} 9.086×10^{3} K
	k_{g3} 1.192
	k_{g4} 2.021×10^{4} m^{-1}
	k_{g5} 0.407
primary nucleation[c,d]	$J_{\mathrm{prim}} = k_{\mathrm{p1}} T \exp\left(-\frac{k_{\mathrm{p2}}}{T}\right) \sqrt{\frac{\rho_c}{c_\star}} (S c_\star)^{7/3} \exp\left(-\frac{k_{\mathrm{p3}} \ln\left(\frac{\rho_c}{c_\star}\right)^3}{\ln(S)^2}\right)$
	k_{p1} 6.412×10^{-7} kg^{-1} s^{-1}
	k_{p2} 1.874×10^{3} K
	k_{p3} 4.300×10^{-3}
secondary nucleation[c,d]	$J_{\mathrm{sec}} = k_{\mathrm{s1}} \exp\left(-\frac{k_{\mathrm{s2}}}{T}\right) (S-1)^{k_{\mathrm{s3}}} (\mu_3)^{k_{\mathrm{s4}}}$
	k_{s1} 2.380×10^{23} kg^{-1} s^{-1}
	k_{s2} 7.677×10^{3} K
	k_{s3} 4.800
	k_{s4} 3.026
dissolution	$D = k_{\mathrm{d}} (S-1)$
	k_{d} 1.00×10^{-6} m s^{-1}
daughter distribution	$d(\lambda, L) = 3L^2(2k_{\mathrm{b1}}+1)\left(\frac{2}{\lambda^3}\right)^{2k_{\mathrm{b1}}+1}\left(L^3 - \frac{\lambda^3}{2}\right)^{2k_{\mathrm{b1}}}$
	k_{b1} 7
breakage rate	$K(L) = k_{\mathrm{b2}} L^{k_{\mathrm{b3}}}$
	k_{b2} 8×10^{-4} kg^{-1} s^{-1}
	k_{b3} 1
shape factor, k_v	0.122
crystal density, ρ_c	1250 kg m^{-3}

[a] All expressions made consistent with dimensions used in this paper.
[b] Expression fitted through data points reported by Sapoundjiev et al. [34].
[c] Simplified from original expression reported in Qamar et al. [24].
[d] Note that $J = J_{\mathrm{prim}} + J_{\mathrm{sec}}$.

Table 2: Specification of processing parameters for case study 1

Quantity	**Value**
m_{C1}	10 kg
m_{M1}	1 kg
T_{C1}	283 K
T_{M1}	298 K
$\dot{m}_{\mathrm{SC1}}$	1×10^{-3} kg s^{-1}
w^{R}_{SC1}	0.2
w^{S}_{SC1}	0.2
$\dot{m}_{\mathrm{C1M1}}$	3×10^{-3} kg s^{-1}
$\dot{m}_{\mathrm{C1F1}}$	7.63×10^{-3} kg s^{-1}
$\dot{m}_{\mathrm{C1C2}}$	2.21×10^{-1} kg s^{-1}

Table 3: Specification of processing parameters for simulations involving enriched feed streams

Quantity	**Value**
m_{C1}	10 kg
m_{M1}	1 kg
m_{C2}	$s\, m_{\mathrm{C1}}$
m_{M2}	$s\, m_{\mathrm{M1}}$
T_{C1}	283 K
T_{M1}	298 K
T_{C2}	283 K
T_{M2}	298 K
$\dot{m}_{\mathrm{SC1}}$	1×10^{-3} kg s^{-1}
$\dot{m}_{\mathrm{SC2}}$	0 kg s^{-1}
w^{R}_{SC1}	0.2
w^{S}_{SC1}	varies (cf. Eq. (14))
$\dot{m}_{\mathrm{C1M1}}$	3×10^{-3} kg s^{-1}
$\dot{m}_{\mathrm{C2M2}}$	$s\, \dot{m}_{\mathrm{C1M1}}$
$\dot{m}_{\mathrm{C1F1}}$	5.26×10^{-3} kg s^{-1}
$\dot{m}_{\mathrm{C2F2}}$	$s\, \dot{m}_{\mathrm{C1F1}}$
$\dot{m}_{\mathrm{C1C2}}$	$s \times 2.21 \times 10^{-1}$ kg s^{-1} $+ s\, \dot{m}_{\mathrm{SC1}}$
$\dot{m}_{\mathrm{C2C1}}$	$s \times 2.21 \times 10^{-1}$ kg s^{-1}